Volume 49
Number 42
14 November 2020
Pages 14709-15110

Dalton Transactions

An international journal of inorganic chemistry

rsc.li/dalton

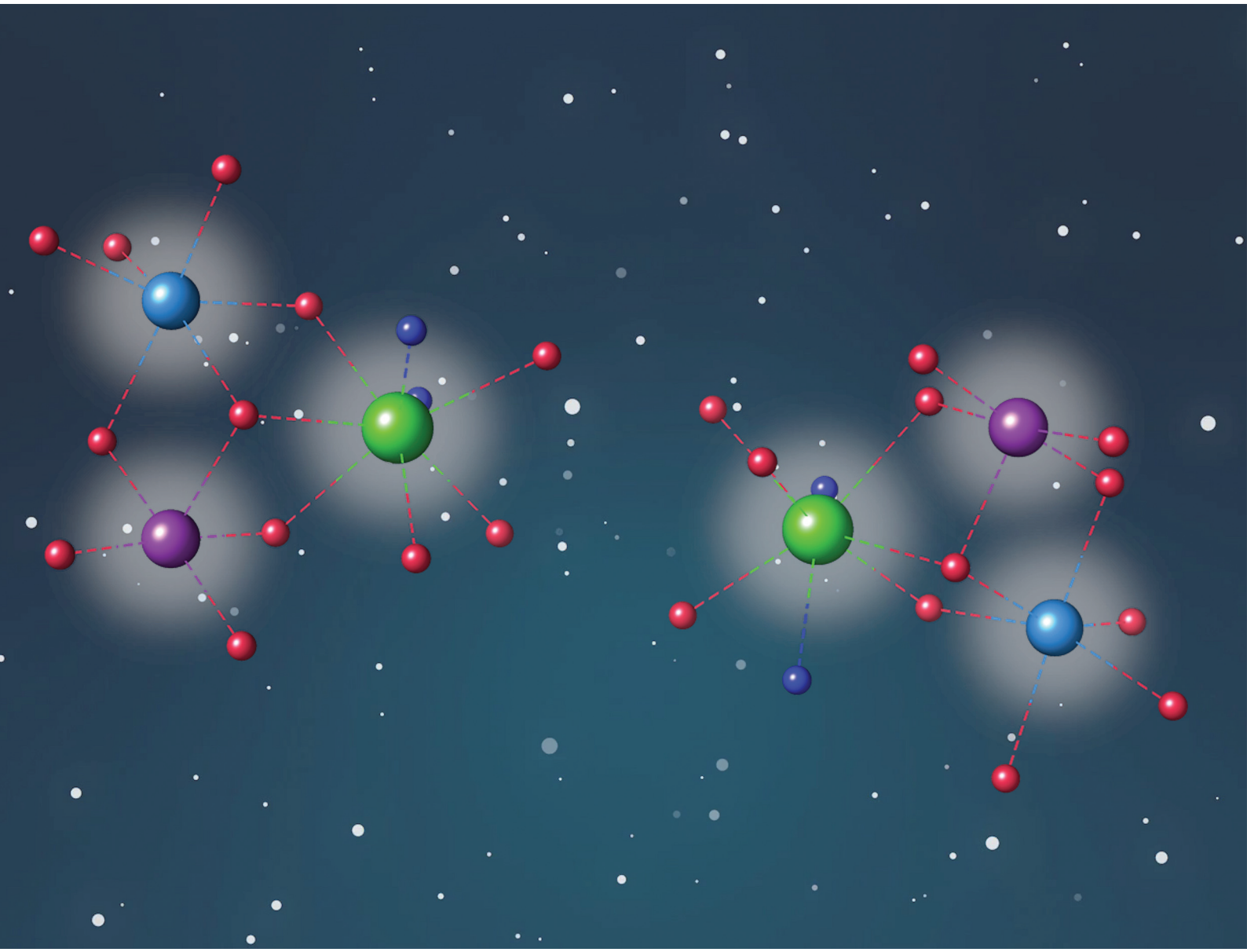

ISSN 1477-9226

ROYAL SOCIETY OF CHEMISTRY

PAPER

Mukesh K. Singh, Euan K. Brechin, Scott J. Dalgarno *et al.*
Magneto-structural studies of an unusual $[Mn^{III}Mn^{II}Gd^{III}(OR)_4]^{4-}$ partial cubane from 2,2′-bis-*p*-^{t}Bu-calix[4]arene

Dalton Transactions

ROYAL SOCIETY OF CHEMISTRY

PAPER

View Article Online
View Journal | View Issue

Check for updates

Cite this: *Dalton Trans.*, 2020, **49**, 14790

Magneto-structural studies of an unusual $[Mn^{III}Mn^{II}Gd^{III}(OR)_4]^{4-}$ partial cubane from 2,2′-bis-*p*-^{t}Bu-calix[4]arene†‡

Marco Coletta, [a,b] Sergio Sanz, [b] Daniel J. Cutler, [b] Simon J. Teat, [c] Kevin J. Gagnon, [c] Mukesh K. Singh, *[b] Euan K. Brechin *[b] and Scott J. Dalgarno *[a]

Received 4th August 2020,
Accepted 7th October 2020

DOI: 10.1039/d0dt02731f

rsc.li/dalton

Reaction of 2,2′-bis-*p*-^{t}Bu-calix[4]arene (H_8L) with $MnCl_2{\cdot}4H_2O$, $GdCl_3{\cdot}6H_2O$ and 2,6-pyridinedimethanol (H_2pdm) affords $[Mn^{III}Mn^{II}Gd^{III}(H_3L)(pdmH)(pdm)(MeOH)_2(dmf)]{\cdot}3MeCN{\cdot}dmf$ (**3**·3MeCN·dmf) upon vapour diffusion of MeCN into the basic dmf/MeOH mother liquor. **3** crystallises in the tetragonal space group $P4_12_12$ with the asymmetric unit comprising the entire cluster. The highly unusual core contains a triangular arrangement of $Mn^{III}Mn^{II}Gd^{III}$ ions housed within a $[Mn^{III}Mn^{II}Gd^{III}(OR)_4]^{4-}$ partial cubane. Magnetic susceptibility and magnetisation data reveal best fit parameters $J_{Mn(II)-Mn(III)}$ = +0.415 cm^{-1}, $J_{Mn(III)-Gd(III)}$ = +0.221 cm^{-1}, $J_{Mn(II)-Gd(III)}$ = −0.258 cm^{-1} and $D_{Mn(III)}$ = −4.139 cm^{-1}. Theoretically derived magnetic exchange interactions, anisotropy parameters, and magneto-structural correlations for **3** are in excellent agreement with the experimental data.

Introduction

Ligand design has always been central to the evolution of molecular magnetism, whether that be in order to manipulate exchange interactions,[1] direct magnetic anisotropy,[2] enhance magnetocalorics,[3] develop quantitative magneto-structural correlations,[4] construct specific topologies,[5] or self-assemble aesthetically pleasing structures – sometimes of enormous nuclearity.[6] Combined with ever-improving technical capabilities and theory, progress in this diverse field continues apace.[7]

p-^{t}Bu-calix[4]arene (TBC[4], molecular framework minus ^{t}Bu groups shown in Fig. 1A) has proven to be a highly versatile ligand for the synthesis of a breadth of polymetallic transition metal (TM), lanthanide metal (LnM) and 3d–4f complexes, in which TM/LnM-TBC[4] moieties act as capping vertices.[8] The TBC[4] polyphenolato pocket is particularly suited to binding the Jahn–Teller (JT) distorted Mn^{III} ion, because it can happily accommodate four short equatorial bonds and two long axial bonds. A good illustration of this comes in the complexes $[Mn^{III}_2Mn^{II}_2(OH)_2(TBC[4])_2(dmf)_6]$ (**1**, Fig. 1B) and $[Mn^{III}_2Mn^{II}Gd^{III}(OH)_2(TBC[4])_2(NO_3)(solvent)_6]$ (**2**, Fig. 1C) whose structures can be considered as two $[Mn^{III}(TBC[4])(OH)$

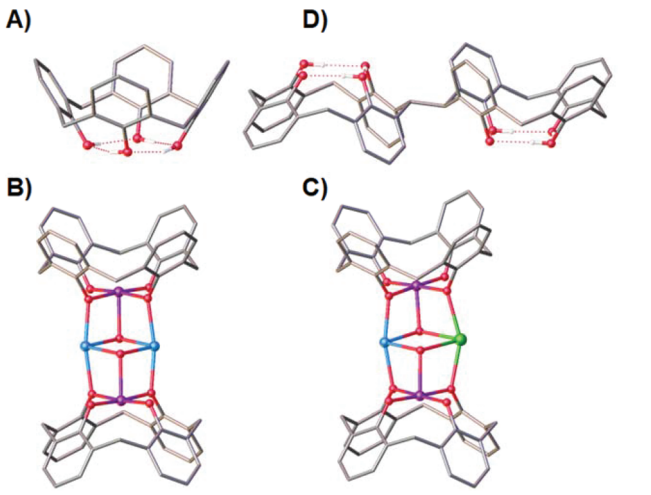

Fig. 1 Single crystal X-ray structures of TBC[4] (A), **1** (B), **2** (C), H_8L (D). Colour code C – grey, O – red, Mn^{II} – pale blue, Mn^{III} – purple, Gd^{III} – green, H - white. Hydrogen atoms (except those involved in lower-rim H-bonding in A and D), ^{t}Bu groups, ligated solvent molecules and co-crystallised solvent/anions omitted for clarity.

[a]*Institute of Chemical Sciences, Heriot-Watt University, Riccarton, Edinburgh, Scotland, EH14 4AS, UK. E-mail: S.J.Dalgarno@hw.ac.uk*
[b]*EastCHEM School of Chemistry, The University of Edinburgh, David Brewster Road, Edinburgh, Scotland, EH9 3FJ, UK. E-mail: ebrechin@ed.ac.uk, mklsingh36@gmail.com*
[c]*Station 11.3.1, Advanced Light Source, Lawrence Berkeley National Laboratory, 1 Cyclotron Road, Berkeley, CA94720, USA*

†Dedicated to Prof. Alan Welch on the occasion of his retirement from Heriot-Watt University.

‡Electronic supplementary information (ESI) available: Bond valence sum calculations, experimental/theoretical figures and tables to support discussion. CCDC 2020261. For ESI and crystallographic data in CIF or other electronic format see DOI: 10.1039/d0dt02731f

(DMF)] metalloligands encapsulating two Mn^{II} ions (**1**) or one Mn^{II} ion and one Gd^{III} ion (**2**).[9]

This general bonding motif has been exploited in the construction of a library of coordination compounds, allowing for the development of detailed empirical metal ion binding rules for TBC[4].[10] Under ambient reaction conditions, TBC[4] preferentially binds TM^{III} ions, will bind TM^{II} ions in the absence of TM^{III} ions, and will bind LnM^{III} ions in the absence of TM^{II} or TM^{III} ions.[11]

One might expect that a systematic move to *p*-^{t}Bu-calix[8]arene would result in ready binding of two Mn^{III} ions, however the nature of the ligand (*e.g.* pleated-loop) means that the polyphenolato pockets do not behave exactly as two TBC[4] equivalents. Instead, this ligand prefers to bind Ln^{III} ions under the standard conditions we employ, though forcing conditions can be used to form Mn-based clusters.[12] Although that is the case, the recent synthesis of TBC[4] molecules modified at one methylene bridge position allows this chemistry to be systematically expanded to include bis-TBC[4] molecules, an important example of which with respect to this paper is 2,2′-bis-*p*-^{t}Bu-calix[4]arene (H_8L, Fig. 1D).[13] This synthetic move to H_8L presents a molecule that truly represents two TBC[4]s as opposed to TBC[8], and a perfect opportunity to translate the aforementioned empirical metal ion binding rules.

The conformational flexibility (ring inversion) of TBC[4] in solution is well known,[14] and in the case of H_8L, presents the possibility of having a ligand with eight phenolic O-atoms in close proximity and, importantly, all converging/oriented in the same direction. This is very attractive from the perspective of polymetallic cluster growth with paramagnetic ions. We have recently begun exploring 3d, 4f and 3d–4f cluster formation with H_8L, and in doing so have reported a range of new clusters with varied nuclearity: $[Mn_8]$, $[Mn_{10}]$, $[Mn_{20}]$, $[Mn_6Gd_2]$, $[Mn_8Gd_2]$, $[Mn_4Gd_4]$, $[Fe_5Gd_4]$, $[Cu_{13}]$ and $[Cu_4Tb_5]$.[15] All of these cases show clear, systematic extension of the empirical metal ion binding rules established for TBC[4]. H_8L has therefore already provided a wealth of new structural chemistry, and shows much promise for the discovery of fascinating new complexes (particularly when one considers the possibility of co-ligand addition, a common approach employed in cluster synthesis). Herein, we outline the synthesis, structure and magnetic behaviour of a new bis-TBC[4]-supported complex, $[Mn^{III}Mn^{II}Gd^{III}(H_3L)(pdmH)(pdm)(MeOH)_2(dmf)]\cdot 3MeCN\cdot dmf$ (**3**·3MeCN·dmf; $pdmH_2$ = 2,6-pyridinedimethanol), together with theoretical magneto-structural studies examining the exchange interactions. The presence of the co-ligand in the resulting assembly breaks our empirical metal ion binding rules, and in doing so affords this new triangular cluster that is of interest from various perspectives.

Results and discussion

Reaction of H_8L with $MnCl_2\cdot 4H_2O$, $GdCl_3\cdot 6H_2O$ and H_2pdm (in the presence of base, Et_3N) affords single crystals of $[Mn^{III}Mn^{II}Gd^{III}(H_3L)(pdmH)(pdm)(MeOH)_2(dmf)]\cdot 3MeCN\cdot dmf$ (**3**·3MeCN·dmf, Fig. 2), upon vapour diffusion of MeCN into the basic dmf/MeOH mother liquor. The crystals were found to be in a tetragonal cell and structure solution was carried out in the space group $P4_12_12$. The ASU comprises the entire cluster, which has a triangular arrangement of $Mn^{III}Mn^{II}Gd^{III}$ ions housed in a $[Mn^{III}Mn^{II}Gd^{III}(OR)_4]^{4-}$ partial cubane. The bis-TBC[4] ligand has undergone conformational change although one of the calixarene binding sites remains unoccupied. This contravenes our established binding rules for this relatively new ligand, and we hypothesise that this is due to the steric constraints enforced by the pdm/pdmH co-ligands that play an important role in directing the prevailing structure.

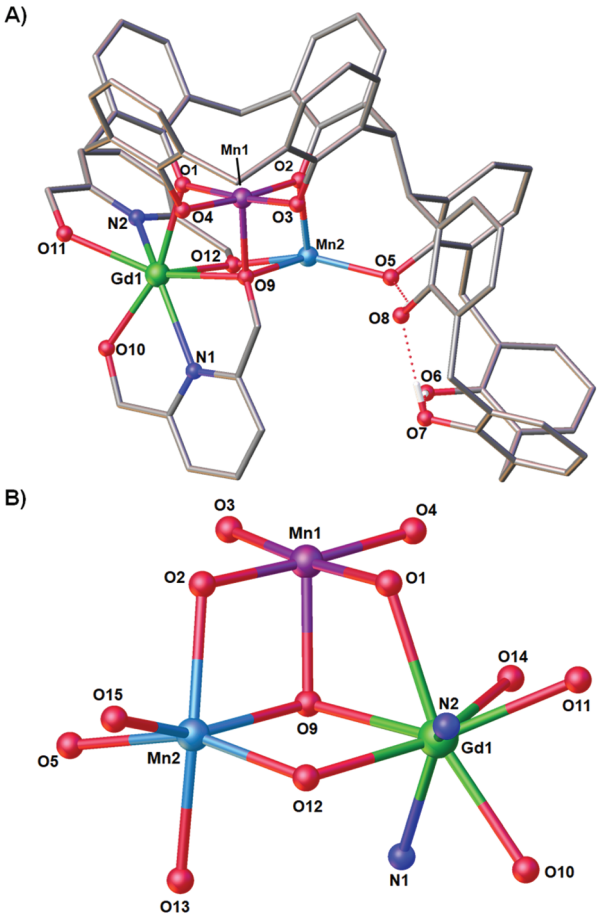

Fig. 2 (A) Single crystal X-ray structure of **3**·3MeCN·dmf and (B) Metallic skeleton of **3**·3MeCN·dmf highlighting the partial cubane arrangement. Selected labels have been added according to discussion. Colour code C – grey, O – red, N – royal blue, Mn^{II} – pale blue, Mn^{III} – purple, Gd^{III} – green, H – white. Hydrogen atoms (except those involved in lower-rim H-bonding), ^{t}Bu groups, ligated solvent molecules and co-crystallised solvent/anions omitted for clarity.

Mn1 is in the trivalent state (Table S1‡) and is bound in a TBC[4] lower-rim tetraphenolato pocket (Mn1–O1–4, 1.873(8)–1.974(9) Å). Its coordination sphere is completed by a μ_3-O atom belonging to the pdm molecule (Mn1–O9, 2.091(8) Å), which is also bonding Mn2 and Gd1 (Mn2–O9, 2.278(8) Å and Gd1–O9, 2.477(8) Å). There is a sixth, longer contact to a MeCN

molecule sitting in the calixarene cavity (Mn1–C020, ~4 Å) and thus one can consider Mn1 as being either square pyramidal or pseudo-octahedral in geometry. Mn2 is in the bivalent state, adopting a distorted octahedral geometry and is located between the two TBC[4] moieties generated through inversion of the ligand. It is bonded to two μ-phenoxides belonging to separate TBC[4] moieties (Mn2–O2, 2.224(8) Å and Mn2–O5, 2.150(8) Å), a μ-O atom of the pdmH molecule (Mn2–O12, 2.097(10) Å), a ligated dmf molecule (Mn2–O15, 2.187(11) Å) and a ligated methanol molecule (Mn2–O13, 2.225(10) Å). Gd1 is octacoordinate, is in a square antiprismatic geometry and is bonded to a phenolic oxygen (Gd1–O1, 2.393(9) Å), a ligated methanol molecule (Gd1–O14, 2.457(10) Å) and the two pdm/H ligands (Gd1–N1, 2.519(12) Å; Gd1–O10, 2.331(9) Å; Gd1–O11, 2.404(9); Gd1–N2, 2.520(12) Å and Gd1–O12, 2.296(10) Å). Structure expansion reveals that the clusters pack *via* H-bonding interactions along the *c* axis, occurring between the protonated and deprotonated OH/O groups of neighbouring H-pdm/pdm molecules (O10···O11′, ~2.47 Å). The shortest metal–metal inter-cluster distance (~5.9 Å) also occurs along the *c* axis, between two neighbouring Gd ions (Fig. 3).

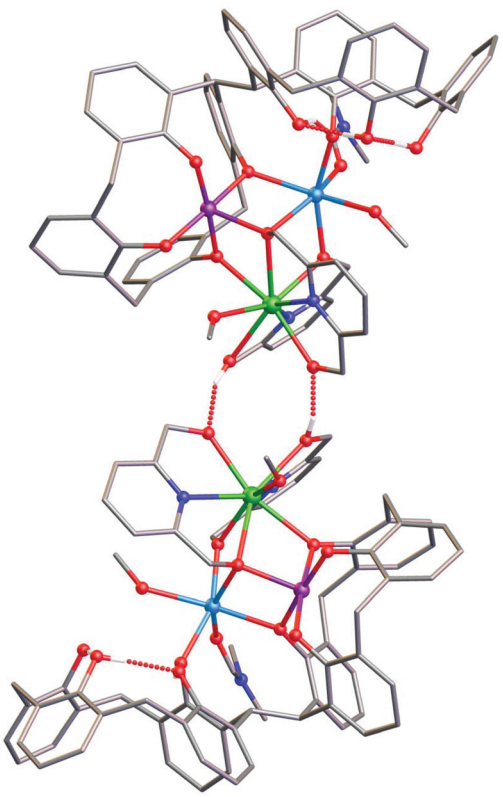

Fig. 3 View orthogonal to the *c* axis in the extended structure of **3** showing the intermolecular hydrogen bonding interaction (dashed red lines). Colour code C – grey, O – red, N – royal blue, Mn^{II} – pale blue, Mn^{III} – purple, Gd^{III} – green, H – white. Hydrogen atoms not involved in H-bonding, ^{t}Bu groups, co-crystallised solvent/anions omitted for clarity.

There are several points of interest to this seemingly rather simple structure. Complex **3** is in fact the first reported example of a heterometallic [Mn_2Gd] triangle containing Mn in the trivalent and bivalent states (Table S1‡). The only other such triangle in the CSD has both Mn ions in the III+ oxidation state.[16] There is also a single [$MnGd_2$] species known, with Mn in the tetravalent state.[17] The triangular [$Mn^{III}Mn^{II}Gd^{III}$] unit in compound **3** is also found in compound **2** and as a moiety in [Mn_8Gd_2].[9] Notably this is the first time that a TBC[4] polyphenolato pocket has ever been found to be unoccupied in our studies on 3d/4f coordination chemistry, and it is also the first example in which the bis-TBC[4] ligand is not fully deprotonated, acting here as a penta- (H_3L) rather than octa-anion (L). As with all our other studies on TBC[4] and bis-TBC[4], the Mn^{III} ion preferentially sits in the polyphenolic pocket and acts as a $[Mn^{III}(TBC[4])]^{-}$ capping fragment/metalloligand.

Magnetic behaviour

The direct current (dc) molar magnetic susceptibility, χ, of a freshly prepared polycrystalline sample of **3** was measured in an applied field, B, of 0.5 T, over the 2–300 K temperature, T, range. The experimental results are showed in Fig. 4, in the form of the $\chi_M T$ product, where $\chi = M/B$, and M is the magnetisation of the sample. At room temperature the $\chi_M T$ product of **3** has a value of 15.0 cm^3 K mol^{-1}, in good agreement with the sum of the Curie constants for non-interacting Mn^{III} (s = 2), Mn^{II} (s = 5/2) and Gd^{III} (s = 7/2) ions, assuming g = 2.00 (15.25 cm^3 k mol^{-1}). As temperature decreases, the $\chi_M T$ product remains essentially invariant to ~50 K before increasing slightly to reach a value of ~15.2 cm^3 K mol^{-1} at T = 20 K, before abruptly decreasing to a value of ~9.0 cm^3 K mol^{-1} at T

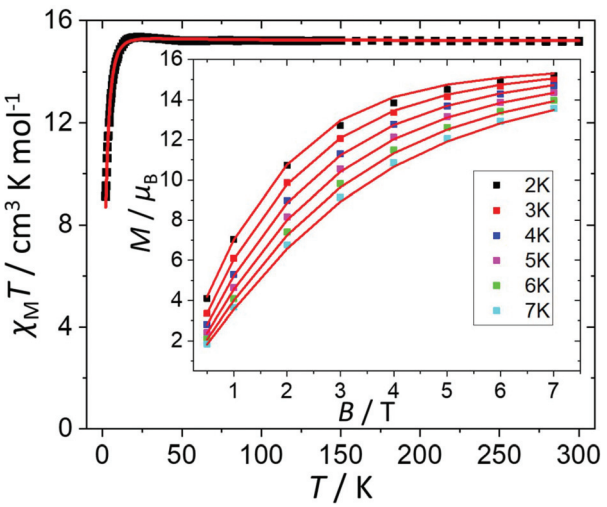

Fig. 4 Plot of $\chi_M T$ *vs.* T in the range T = 2–300 K and B = 0.5 T. Inset: field dependence of the magnetization (M) measured in the T = 2–7 K and B = 0.5–7.0 T temperature and field ranges. The (□) symbols represent the experimental data and the solid red lines the fit of the experimental data to spin-Hamiltonian (1). See text for details.

= 2.0 K. This is clearly indicative of the presence of very weak magnetic exchange interactions. In order to gain more insight into the low temperature energy spectrum of **3**, low temperature variable-temperature-and-variable-field (VTVB) magnetisation data were measured in the temperature range 2–7 K, in magnetic fields from 0.5 to 7.0 T (Fig. 4 inset). At the lowest temperature and highest field, M reaches a value of ~15.2 μ_B. To quantitatively interpret the magnetic properties of **3**, we use the following general spin-Hamiltonian (1):

$$\hat{H} = \sum_i D_i(\hat{S}_{z,i}^2 - S_i(S_i+1)/3) + \mu_B B \sum_i g_i \hat{S}_i - 2\sum_{ij<1} J_{ij}\hat{S}_i \cdot \hat{S}_j \quad (1)$$

where the summation indices i, j run through the constitutive metal centres, D is the uniaxial single-ion anisotropy parameter of Mn^{III}, $\hat{S}$ is a spin operator, S is the total spin and J is the isotropic exchange interaction parameter.

The $\chi_M T$ and VTVB magnetisation data were simultaneously fitted to spin-Hamiltonian (1) using the program PHI assuming three different exchange interactions in the $[Mn^{III}Mn^{II}Gd^{III}]$ triangle.[18] This results in the following best fit (error) parameters: $J_{Mn(II)-Mn(III)}$ = +0.415 (1.4×10^{-2}) cm^{-1}, $J_{Mn(III)-Gd(III)}$ = +0.221 (5.7×10^{-3}) cm^{-1}, $J_{Mn(II)-Gd(III)}$ = −0.258 (3.8×10^{-3}) cm^{-1} and $D_{Mn(III)}$ = −4.139 (4.8×10^{-2}) cm^{-1}, with the g-factors fixed at g = 2.00 for Mn^{II} and Gd^{III} and g = 1.98 for Mn^{III}. Therefore, the Mn^{III}–Mn^{II} interaction and the Mn^{III}–Gd^{III} interaction are very weakly ferromagnetic and the Mn^{II}–Gd^{III} interaction is very weakly antiferromagnetic. These parameters are similar to those found for complex **2**.[9] With these parameters the ground spin-state of **3**, when only the isotropic part of spin-Hamiltonian (1) is taken into account, is an S = 4 spin-state, lying very close to several excited spin states (Fig. 5).

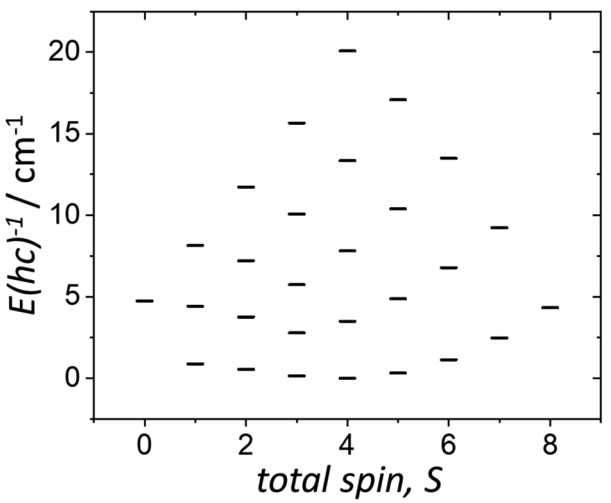

Fig. 5 Energy spectrum of **3** at zero magnetic field, for the isotropic part of spin-Hamiltonian (1), with the determined best-fit parameters, as described in the text.

Theoretical studies

To understand the origin of the magnetic exchange interactions in more detail we have performed *ab initio* calculations on a model complex, **3A** (Fig. S1‡), using the MOLCAS 8.0 suite.[19] Model **3A** has the same structure as **3**, but with the terminal ^{t}Bu groups on the calixarene ligand replaced with Me groups to reduce computational cost.

We have first performed *ab initio* CASSCF[20]/RASSI-SO[21]/SINGLE_ANISO[22] calculations on the individual paramagnetic ions. The Mn^{III} centre shows moderate easy-axis anisotropy (D = −3.3 cm^{-1}, E = 0.1 cm^{-1}, $g_{xx}/g_{yy}/g_{zz}$ = 1.99/1.99/1.96), whereas the other two paramagnetic centres, Gd^{III} and Mn^{II}, are found to be isotropic ($g_{xx} = g_{yy} = g_{zz}$ = 2.00). These values are as expected, and in accordance with the experimental values. Next, we have performed POLY_ANISO calculations, which includes the Lines model, to estimate the magnetic coupling constants.[23] The so-obtained exchange interactions are given in Table 1 and are in good agreement with the experimental values and simulate the susceptibility data well (Fig. 6a). The $J_{Mn(II)-Mn(III)}$ and $J_{Mn(III)-Gd(III)}$ interactions are found to be weakly ferromagnetic, whereas $J_{Mn(II)-Gd(III)}$ is found to be weakly antiferromagnetic. It is worth noting that for both $J_{Mn(II)-Gd(III)}$ and $J_{Mn(III)-Gd(III)}$ the dipolar contribution is calculated to be dominant, as seen previously for other 3d–4f complexes.[24]

To further confirm the magnetic exchange values, we have performed density functional theory (DFT) calculations in the G09 suite using two different methods (see computational details section for more information).[25] In the first method, we have performed calculations on model **3A**. In the second method, we have performed pairwise exchange interaction calculations on model complexes containing only two paramagnetic centres, replacing the third paramagnetic centre with a diamagnetic element, *i.e.* $Gd^{III}/Mn^{III}/Mn^{II}$ with $Y^{III}/Ga^{III}/Zn^{II}$, respectively (Fig. S1(b)–(d)).‡ The computed magnetic exchange values from both methods are in good agreement with the *ab initio* calculated values (Table 1).

The spin densities for model **3A** (Fig. 6(b) and (c), Fig. S2‡) reveal that while dominant spin delocalisation is observed for both the Mn^{III} (3.981) and Mn^{II} (4.790) ions, spin polarisation is detected for Gd^{III} (7.038). The μ_3-bridging O-atom (O9, Fig. 2) has a spin density of 0.110, more than three times higher than any other bridging atoms in the molecule, and is therefore expected to play a dominant role in the magnetic

Table 1 *Ab initio* POLY_ANISO derived magnetic exchange interaction parameters in **3**. The values in parentheses are calculated from DFT. The bold values are calculations performed on model complex **3A** shown in Fig. S1(a).‡ The italised values are the pairwise exchange interactions calculated on the model complexes shown in Fig. S1(b)–(d) in which the Mn^{III}, Mn^{II} and Gd^{III} ions are, in turn, replaced with the diamagnetic Ga^{III}, Zn^{II} and Y^{III} ions

	J^{total}/cm^{-1}	$J^{exchange}/cm^{-1}$	$J^{dipolar}/cm^{-1}$
$J_{Mn(II)-Mn(III)}$	+0.50	+0.52 (**1.04**/*1.10*)	−0.02
$J_{Mn(III)-Gd(III)}$	+0.10	−0.12 (**−0.08**/*−0.08*)	+0.22
$J_{Mn(II)-Gd(III)}$	−0.16	+0.08 (**0.12**/*0.14*)	−0.24

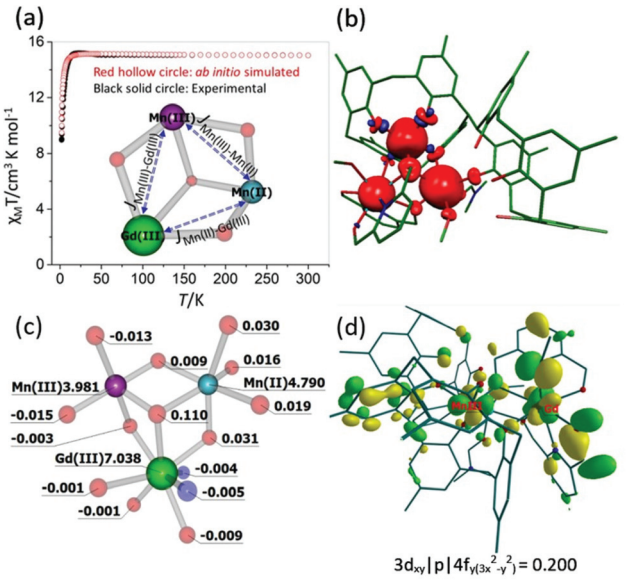

Fig. 6 (a) *Ab initio* simulated, temperature dependent $\chi_M T$ *versus* T data for **3**. The solid black circles are the experimental data and the hollow red circles the *ab initio* derived data. The core structure of **3** with magnetic coupling scheme is shown in the inset. (b) and (c) DFT computed spin density plot together with spin density values on selected atoms for model **3A**. (d) Representative molecular orbital showing the $3d_{xy}|p|4f_{y(3x^2-y^2)}$ interaction for Mn^{III}–Gd^{III} pair. See Table S2‡ for the computed overlap integral values for the Mn^{II}–Gd^{III}, Mn^{II}–Gd^{II} and Mn^{II}–Mn^{III} pairs.

superexchange. It is also worth mentioning here that the *p*-Me groups, which we have used in place of the ^{t}Bu groups in **3A** have a spin density very close to zero, suggesting the model to be reliable.

Previous studies performed on 3d–4f complexes have emphasised the importance of the 3d orbitals of the transition metals in controlling the two possible contributions (J_F and J_{AF}) to the total magnetic exchange interaction.[26] The first contribution, J_F, where partial electron transfer occurs from the 3d orbitals of the Mn^{III}/Mn^{II} ions to the empty 5d/6s orbitals of Gd^{III} ion, adds to the ferromagnetic part of the magnetic exchange interaction. The larger the charge transfer the larger the ferromagnetic contribution. The second contribution, J_{AF}, arises from overlap between the non-orthogonal, singly occupied molecular orbitals (SOMOs) of the 3d ion with the half-filled 4f orbitals of the Gd^{III} ions. The former contribution to the magnetic exchange interaction can be estimated using natural bonding orbital (NBO) analysis which investigates the charge transfer, whereas the latter contribution can be estimated by performing overlap integral calculations. For $J^{exchange}_{Mn(II)–Gd(III)}$, all the overlap integral values are small leading to a small ferromagnetic exchange interaction (Table S2‡). For $J^{exchange}_{Mn(III)–Gd(III)}$, one overlap integral value is estimated to be relatively strong ($3d_{xy}|p|4f_{y(3x^2-y^2)}$, Fig. 6d) leading to a small antiferromagnetic exchange interaction. This is opposite to that obtained from the experimental fit, though we note the absolute magnitide of the difference is extremely small. Larger charge transfer from $Mn^{II}(3d) \rightarrow Gd^{III}(6s/5d)$ compared to $Mn^{III}(3d) \rightarrow Gd^{III}(6s/5d)$ further supports this. For $J^{exchange}_{Mn(II)–Gd(III)}$ all the overlap integral values are estimated to be small leading to a small ferromagnetic exchange interaction.

To investigate these interactions a little further, we have performed a magneto-structural correlation by varying the Mn^{III}/Mn^{II}–O–Gd^{III} angle, the $Mn^{III/II}/Gd^{III}$–O distance and the $Mn^{III/II}$–O–Gd^{III}–O dihedral angle on bimetallic model complexes designed from complex **3**. The models $\mathbf{3}_{Mn(II)–Gd(III)}$ and $\mathbf{3}_{Mn(III)–Gd(III)}$ are shown in Fig. 7(a) and (b), respectively. The sign and magnitude of $J^{exchange}_{Mn(II)–Gd(III)}$ and $J^{exchange}_{Mn(III)–Gd(III)}$ are in good agreement with those in Table 1 (+0.26 cm^{-1} and −0.22 cm^{-1}, respectively). Magneto-structural correlations developed for $J^{exchange}_{Mn(II)–Gd(III)}$ and $J^{exchange}_{Mn(III)–Gd(III)}$ suggest that the Mn^{III}/Mn^{II}–O–Gd^{III} angle is the most dominant structural parameter (Fig. 7(c) and (d), Fig. S3‡). At smaller angles the antiferromagnetic interaction is favoured, at the larger angles the ferromagnetic interaction is favoured. This is as expected, since at smaller angles larger overlap between the Gd(4f) and $Mn^{II/III}$(3d) orbitals are observed, diminishing with increasing angle (Fig. S4, Tables S3 and S4‡). These findings are in agreement with previous theoretical studies on di-, tri- and tetranuclear Mn^{III}–Gd^{III} cluster compounds.[26]

In search of models representing $J^{exchange}_{Mn(II)–Mn(III)}$, we have developed two different models ($\mathbf{3}_{Mn(II)–Mn(III)}$ − 1 and $\mathbf{3}_{Mn(II)–Mn(III)}$ − 2, Fig. S5‡). In both models the rigidity provided by the 2,2′-bis-*p*-^{t}Bu-calix[4]arene ligand needs to be removed in order to obtain a model whereby structural parameters can be fine-tuned. However, as soon as we remove H_8L, the sign of the magnetic exchange interaction switches from ferromagnetic to antiferromagnetic (Fig. S5‡) due to presence of two strong magnetic orbital overlaps ($Mn(II)d_{yz}|p|Mn(III)d_{z^2}$

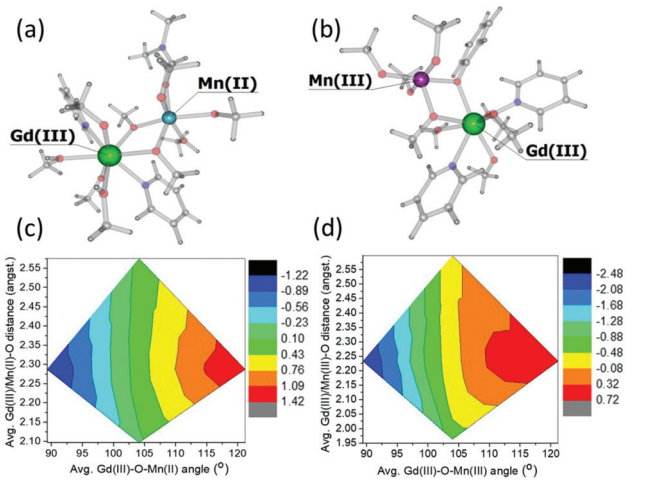

Fig. 7 Models $\mathbf{3}_{Mn(II)–Gd(III)}$ (a) and $\mathbf{3}_{(Mn(III)–Gd(III)}$ (b) together with the magneto-structural correlation contour plots (c) and (d) performed by varying the average Mn^{II}/Mn^{III}–O–Gd^{III} angle and average $Mn^{III/II}/Gd^{III}$–O distance with respect to the magnetic exchange coupling constants $J^{exchange}_{Mn(II)–Gd(III)}$ and $J^{exchange}_{Mn(III)–Gd(III)}$. The keys represents the magntidue of the exchange, ranging from most antiferromagnetic (black) to most ferromagnetic (red). For both models, the change in the magnitude of the interaction with respect to the change in $Mn^{III/II}$–O–Gd^{III}–O dihedral angle is minimal. See Fig. S3 of the ESI for more details.‡

and Mn(II)$d_{x^2-y^2}$|p|Mn(III)d_{z^2} for $\mathbf{3}_{Mn(II)-Mn(III)}$ − 1 and Mn(II)d_{yz}|p|Mn(III)d_{z^2} and Mn(II)d_{xz}|p|Mn(III)d_{z^2} for $\mathbf{3}_{Mn(II)-Mn(III)}$ − 2, Table S5, Fig. S6 and 7‡). Although this renders any further investigation moot, the above does highlight both the structural and magnetic importance of the calixarene ligand. Ligand rigidity is rarely a consideration in design criteria when contemplating the nature of magnetic exchange. Considering the bond angles and distances in **3** in tandem with previous magneto-structural studies developed for a variety of Mn^{III}–Mn^{II} species, would infer a small ferromagnetic interaction being present in complex **3**, in agreement with our calculated $J^{exchange}_{Mn(II)-Mn(III)}$ value.[27]

Conclusions

Reaction of bis-TBC[4] with $MnCl_2{\cdot}4H_2O$, $GdCl_3{\cdot}6H_2O$ and H_2pdm results in the formation of the complex $[Mn^{III}Mn^{II}Gd^{III}(H_3L)(pdmH)(pdm)(MeOH)_2(dmf)]$ (**3**) whose structure describes a triangular arrangement of $Mn^{III}Mn^{II}Gd^{III}$ ions housed in a $[Mn^{III}Mn^{II}Gd^{III}(OR)_4]^{4-}$ partial cubane. Although the bis-TBC[4] has undergone conformational change as the penta-anion (Fig. 2A), one lower-rim pocket remains unoccupied which is likely due to the steric constraints enforced by the co-ligands. Compound **3** is the first example of a heterometallic $[Mn_2Gd]$ triangle containing Mn in the trivalent and bivalent states, although this unit has previously been observed within the larger species $[Mn^{III}_2Mn^{II}Gd^{III}]$ (**2**) and $[Mn_8Gd_2]$, constructed from TBC[4] and bis-TBC[4], respectively. Susceptibility and magnetisation data reveal very weak exchange interactions between the constituent metal centres, with best fit parameters $J_{Mn(II)-Mn(III)}$ = +0.415 (1.4×10^{-2}) cm^{-1}, $J_{Mn(III)-Gd(III)}$ = +0.221 (5.7×10^{-3}) cm^{-1}, $J_{Mn(II)-Gd(III)}$ = −0.258 (3.8×10^{-3}) cm^{-1} and $D_{Mn(III)}$ = −4.139 (4.8×10^{-2}) cm^{-1}, consistent with those seen in $[Mn^{III}2Mn^{II}Gd^{III}]$ (**2**). *Ab initio* calculated magnetic exchange interactions, anisotropy parameters, and theoretical magneto-structural correlations for **3** are found to be in excellent agreement with the experimental data, highlighting the importance of Mn^{III}/Mn^{II}–O–Gd^{III} angles and the rigidity of the 2,2′-bis-*p*-^{t}Bu-calix[4]arene (H_8L) ligand in governing the sign and magnitude of the exchange interactions.

Experimental section

H_8L was synthesised according to literature procedure.[13]

Synthesis of $[Mn^{III}Mn^{II}Gd^{III}(H_3L)(pdmH)(pdm)(MeOH)_2(dmf)]{\cdot}3MeCN{\cdot}dmf$, 3·3MeCN·dmf

H_8L (150 mg, 0.116 mmol), $MnCl_2{\cdot}4H_2O$ (23 mg, 0.116 mmol), $GdCl_3{\cdot}6H_2O$ (35 mg, 0.116 mmol) and $pdmH_2$ (32.2 mg, 0.232 mmol) were suspended in a 1 : 1 dmf/MeOH mixture (20 mL) and stirred for 10 minutes. Et_3N (0.15 mL) was added and the resulting purple solution was stirred for additional 2 hours and then filtered. The mother liquor was allowed to slowly diffuse with acetonitrile vapours, affording dark purple crystals suitable for X-ray diffraction studies. Elemental analysis (%) calculated for **1**, $C_{116}H_{151}Mn_2GdN_7O_{16}$ (M = 2166.6): C, 64.31%; H, 7.02%; N, 4.53%. Found: C, 64.24%; H, 6.83%; N, 4.23%. Yield 51 mg (20.3%). Crystal data for **3** (CCDC 2020261‡): $C_{116}H_{151}Mn_2GdN_7O_{16}$, M = 2166.6, 0.3 × 0.03 × 0.01 mm^3, tetragonal, space group $P4_12_12$ (no. 92), a = 23.2275(8) Å, c = 44.2459(18) Å, V = 23 871.4(19) $Å^3$, Z = 8, Bruker D8 diffractometer equipped with a PHOTON 100 detector, synchrotron radiation, λ = 0.7749 Å, T = 100(15) K, $2\theta_{max}$ = 48.852°, 151 662 reflections collected, 15 095 unique (R_{int} = 0.0531). Final GooF = 1.037, $R1$ = 0.0854, w$R2$ = 0.1763.

Computational details

We have performed *ab initio* CASSCF[20]/RASSI-SO[21]/SINGLE_ANISO[22] calculations on a model complex, **3A**, made from the X-ray structure to estimate the magnetic coupling constants in complex **3** using the MOLCAS 8.0 suite.[19] We have considered each paramagnetic ion separately by keeping the ions of interest and substituting the third paramagnetic ion with a diamagnetic ion, *i.e.* $Gd^{III}/Mn^{III}/Mn^{II}$ with $Y^{III}/Ga^{III}/Zn^{II}$. We have used the H.ANO-RCC...2s., C.ANO-RCC...3s2p., N.ANO-RCC...3s2p., O.ANO-RCC...3s2p1d., Mn.ANO-RCC...5s4p2d1f., Zn.ANO-RCC...5s4p2d., Ga.ANO-RCC...5s4p1d., Y.ANO-RCC...6s5p3d., Gd.ANO-RCC...7s6p4d2f1g basis sets.[28] During CASSCF calculations for a single Gd^{III} ion, we have used seven electrons in seven active 4f orbitals. For the Mn^{III} and Mn^{II} ions we have used four and five electrons, respectively, in five active 3d orbitals. Next, in the RASSI-SO step for the Gd^{III} ion, we have used 1, 48 and 76 roots for the octet, sextet and quartet spin multiplicities. For the Mn^{III} ion, 5, 45 and 50 roots for quintet, triplet and singlet spin multiplicities have been used, respectively. For the Mn^{II} ion, 1, 24 and 75 roots for sextet, quartet and doublet spin multiplicities have been used, respectively.[24,29] The resultant spin–orbit multiplets have been used further to estimate local magnetic properties *via* the SINGLE_ANISO approach.[22] The magnetic exchange interactions (Js) have been computed between all paramagnetic ions for all complexes by fitting *ab initio* POLY_ANISO with the experimental data.[23a]

We have also used the G09 programme on model complex **3A** to estimate the magnetic coupling constant.[25] Noodlemann's broken symmetry[30] together with the B3LYP functional[31] is known to be a reliable approach to estimate magnetic exchange coupling constants.[32] We have used the relativistically corrected effective core potential (ECP) basis set of Cundari and Stevens (CSDZ) for the Gd^{III} ion,[33] Ahlrichs-TZV basis set for the Mn ions,[34] and the 6-31G** basis set for O, N, C and H atoms.[35] We have computed four spin configurations to estimate three possible exchange coupling constants. The computed spin configurations include a high spin configuration with all spins up and three other configurations with one of the spin centres down. We have used the same methodology mentioned earlier for performing natural bonding orbitals (NBOs) analysis to investigate the charge transfer.[32d,e]

Conflicts of interest

There are no conflicts to declare.

Acknowledgements

We thank the EPSRC for financial support under grant reference numbers EP/I03255X/1 and EP/I031421/1, and the Marie Skłodowska-Curie actions (MSCA) for grant MMQIP 832488 (to MKS). We also thank Heriot-Watt University for financial support for M. C. through the James-Watt Scholarship programme. This research used resources of the Advanced Light Source, a U.S. DOE Office of Science User Facility under contract no. DE-AC02-05CH11231.

Notes and references

1 (*a*) O. Kahn, P. Tola, J. Galy and H. Coudanne, *J. Am. Chem. Soc.*, 1978, **100**(12), 3931; (*b*) T. Mallah, A. Marvilliers and E. Rivière, *Philos. Trans. R. Soc., A*, 1999, **357**, 3139.

2 (*a*) M. Murrie, *Chem. Soc. Rev.*, 2010, **39**, 1986; (*b*) J. D. Rinehart and J. R. Long, *Chem. Sci.*, 2011, **2**, 2078–2085.

3 (*a*) G. Lorusso, O. Roubeau and M. Evangelisti, *Angew. Chem., Int. Ed.*, 2016, **55**, 3360; (*b*) G. Lorusso, E. Natividad, M. Evangelisti and O. Roubeau, *Mater. Horiz.*, 2019, **6**, 144.

4 (*a*) H. Weihe and H.-U. Güdel, *J. Am. Chem. Soc.*, 1998, **120**(12), 2870; (*b*) C. J. Milios, R. Inglis, A. Vinslava, R. Bagai, W. Wernsdorfer, S. Parsons, S. P. Perlepes, G. Christou and E. K. Brechin, *J. Am. Chem. Soc.*, 2007, **129**, 12505.

5 (*a*) L. N. Dawe, K. V. Shuvaev and L. K. Thompson, *Inorg. Chem.*, 2009, **48**, 3329; (*b*) E. Garlatti, T. Guidi, S. Ansbro, P. Santini, G. Amoretti, J. Ollivier, H. Mutka, G. Timco, I. Vitorica-Yrezabal, G. Whitehead, R. E. P. Winpenny and S. Carretta, *Nat. Commun.*, 2017, **8**, 14543; (*c*) M. S. Fataftah and D. E. Freedman, *Chem. Commun.*, 2018, **54**, 13773.

6 (*a*) X.-Y. Zheng, Y.-H. Jiang, G.-L. Zhuang, D.-P. Liu, H.-G. Liao, X.-J. Kong, L.-S. Long and L.-S. Zheng, *J. Am. Chem. Soc.*, 2017, **139**, 18178; (*b*) W.-P. Chen, P.-Q. Liao, P.-B. Jin, L. Zhang, B.-K. Ling, S.-C. Wang, Y.-T. Chan, X.-M. Chen and Y.-Z. Zheng, *J. Am. Chem. Soc.*, 2020, **142**, 4663.

7 (*a*) E. Garlatti, L. Tesi, A. Lunghi, M. Atzori, D. J. Voneshen, P. Santini, S. Sanvito, T. Guidi, R. Sessoli and S. Carretta, *Nat. Commun.*, 2020, **11**, 1751; (*b*) T. Gupta and G. Rajaraman, *Chem. Commun.*, 2016, **52**, 8972; (*c*) J. Schnack, *Dalton Trans.*, 2010, **39**, 4677.

8 M. Coletta, E. K. Brechin and S. J. Dalgarno, Structural Trends in Calix[4]arene-Supported Cluster Chemistry, in *Calixarenes and Beyond*, ed. P. Neri, J. Sessler and M.-X. Wang, Springer International Publishing, 2016, pp. 671–689.

9 (*a*) G. Karotsis, S. J. Teat, W. Wernsdorfer, S. Piligkos, S. J. Dalgarno and E. K. Brechin, *Angew. Chem., Int. Ed.*, 2009, **48**, 8285; (*b*) S. M. Taylor, G. Karotsis, R. D. McIntosh, S. Kennedy, S. J. Teat, C. M. Beavers, W. Wernsdorfer, S. Piligkos, S. J. Dalgarno and E. K. Brechin, *Chem. – Eur. J.*, 2011, **17**, 7521; (*c*) M. A. Palacios, R. McLellan, C. M. Beavers, S. J. Teat, H. Weihe, S. Piligkos, S. J. Dalgarno and E. K. Brechin, *Chem. – Eur. J.*, 2015, **21**, 11212.

10 (*a*) C. Aronica, G. Chastanet, E. Zueva, S. A. Borshch, J. M. Clemente-Juan and D. Luneau, *J. Am. Chem. Soc.*, 2008, **130**, 2365; (*b*) G. Karotsis, M. Evangelisti, S. J. Dalgarno and E. K. Brechin, *Angew. Chem., Int. Ed.*, 2009, **48**, 9928; (*c*) G. Karotsis, S. Kennedy, S. J. Teat, C. M. Beavers, D. A. Fowler, J. J. Morales, M. Evangelisti, S. J. Dalgarno and E. K. Brechin, *J. Am. Chem. Soc.*, 2010, **132**, 12983; (*d*) S. Sanz, K. Ferreira, R. D. McIntosh, S. J. Dalgarno and E. K. Brechin, *Chem. Commun.*, 2011, **47**, 9042; (*e*) S. Sanz, R. D. McIntosh, C. M. Beavers, S. J. Teat, M. Evangelisti, E. K. Brechin and S. J. Dalgarno, *Chem. Commun.*, 2012, **48**, 1449; (*f*) G. Karotsis, S. Kennedy, S. J. Dalgarno and E. K. Brechin, *Chem. Commun.*, 2010, **46**, 3884.

11 (*a*) M. Coletta, S. Sanz, E. K. Brechin and S. J. Dalgarno, *Chemistry*, 2020, **2**, 253.

12 S. Du, H. Ke, Y. Bi, H. Tan, Y. Yu, J. Tang and W. Liao, *Inorg. Chem. Commun.*, 2013, **29**, 85.

13 L. T. Carroll, P. A. Hill, C. Q. Ngo, K. P. Klatta and J. L. Fantini, *Tetrahedron*, 2013, **69**, 5002.

14 I. Thondorf, in *Calixarenes 2001*, Kluwer Academic, Dordrecht, 2001, ch. 15.

15 (*a*) R. McLellan, M. A. Palacios, C. M. Beavers, S. J. Teat, S. Piligkos, E. K. Brechin and S. J. Dalgarno, *Chem. – Eur. J.*, 2015, **21**, 2804; (*b*) M. Coletta, R. McLellan, A. Waddington, S. Sanz, K. J. Gagnon, S. J. Teat, E. K. Brechin and S. J. Dalgarno, *Chem. Commun.*, 2016, **52**, 14246; (*c*) M. Coletta, R. McLellan, S. Sanz, K. J. Gagnon, S. J. Teat, E. K. Brechin and S. J. Dalgarno, *Chem. – Eur. J.*, 2017, **23**, 14073; (*d*) M. Coletta, S. Sanz, L. J. McCormick, S. J. Teat, E. K. Brechin and S. J. Dalgarno, *Dalton Trans.*, 2017, **46**, 16807.

16 S. Mukherjee, M. R. Daniels, R. Bagai, K. A. Abboud, G. Christou and C. Lampropoulos, *Polyhedron*, 2010, **29**, 54.

17 C. Lampropoulos, T. C. Stamatatos, K. A. Abboud and G. Christou, *Inorg. Chem.*, 2009, **48**, 429.

18 N. F. Chilton, R. P. Anderson, L. D. Turner, A. Soncini and K. S. Murray, *J. Comput. Chem.*, 2013, **34**, 1164.

19 (*a*) F. Aquilante, J. Autschbach, R. K. Carlson, L. F. Chibotaru, M. G. Delcey, L. De Vico, I. F. Galván, N. Ferré, L. M. Frutos, L. Gagliardi, M. Garavelli, A. Giussani, C. E. Hoyer, G. Li Manni, H. Lischka, D. Ma, P. Å. Malmqvist, T. Müller, A. Nenov, M. Olivucci, T. B. Pedersen, D. Peng, F. Plasser, B. Pritchard, M. Reiher, I. Rivalta, I. Schapiro, J. Segarra-Martí,M. Stenrup, D. G. Truhlar, L. Ungur, A. Valentini,S. Vancoillie, V. Veryazov, V. P. Vysotskiy, O. Weingart, F. Zapata and

R. Lindh, *J. Comput. Chem.*, 2015, **37**, 506–541; (*b*) F. Aquilante, L. De Vico, N. Ferré, G. Ghigo, P.-å. Malmqvist, P. Neogrády, T. B. Pedersen, M. Pitoňák, M. Reiher, B. O. Roos, L. Serrano-Andrés, M. Urban, V. Veryazov and R. Lindh, *J. Comput. Chem.*, 2010, **31**, 224–247; (*c*) J. A. Duncan, *J. Am. Chem. Soc.*, 2009, **131**, 2416–2416; (*d*) V. Veryazov, P. O. Widmark, L. Serrano-Andrés, R. Lindh and B. O. Roos, *Int. J. Quantum Chem.*, 2004, **100**, 626–635; (*e*) G. Karlström, R. Lindh, P.-Å. Malmqvist, B. O. Roos, U. Ryde, V. Veryazov, P.-O. Widmark, M. Cossi, B. Schimmelpfennig, P. Neogrady and L. Seijo, *Comput. Mater. Sci.*, 2003, **28**, 222–239.

20 B. Swerts, L. F. Chibotaru, R. Lindh, L. Seijo, Z. Barandiaran, S. Clima, K. Pierloot and M. F. A. Hendrickx, *J. Chem. Theory Comput.*, 2008, **4**, 586–594.

21 P. Å. Malmqvist, B. O. Roos and B. Schimmelpfennig, *Chem. Phys. Lett.*, 2002, **357**, 230–240.

22 (*a*) L. F. Chibotaru and L. Ungur, *J. Chem. Phys.*, 2012, **137**, 064112; (*b*) L. F. Chibotaru, A. Ceulemans and H. Bolvin, *Phys. Rev. Lett.*, 2008, **101**, 033003.

23 (*a*) M. E. Lines, *J. Chem. Phys.*, 1971, **55**, 2977; (*b*) L. Ungur and L. F. Chibotaru, *POLY_ANISO program*, 2007.

24 (*a*) Y. Peng, M. K. Singh, V. Mereacre, C. E. Anson, G. Rajaraman and A. K. Powell, *Chem. Sci.*, 2019, **10**, 5528–5538; (*b*) D. Basak, J. v. Leusen, T. Gupta, P. Kögerler, V. Bertolasi and D. Ray, *Inorg. Chem.*, 2020, **59**, 2387–2405.

25 M. J. Frisch, G. W. Trucks, H. B. Schlegel, G. E. Scuseria, M. A. Robb, J. R. Cheeseman, G. Scalmani, V. Barone, B. Mennucci, G. A. Petersson, H. Nakatsuji, M. Caricato, X. Li, H. P. Hratchian, A. F. Izmaylov, J. Bloino, G. Zheng, J. L. Sonnenberg, M. Hada, M. Ehara, K. Toyota, R. Fukuda, J. Hasegawa, M. Ishida, T. Nakajima, Y. Honda, O. Kitao, H. Nakai, T. Vreven, J. A. Montgomery, J. E. Peralta, F. Ogliaro, M. Bearpark, J. J. Heyd, E. Brothers, K. N. Kudin, V. N. Staroverov, R. Kobayashi, J. Normand, K. Raghavachari, A. Rendell, J. C. Burant, S. S. Iyengar, J. Tomasi, M. Cossi, N. Rega, J. M. Millam, M. Klene, J. E. Knox, J. B. Cross, V. Bakken, C. Adamo, J. Jaramillo, R. Gomperts, R. E. Stratmann, O. Yazyev, A. Austin, J. R. Cammi, C. Pomelli, J. W. Ochterski, R. L. Martin, K. Morokuma, V. G. Zakrzewski, G. A. Voth, P. Salvador, J. J. Dannenberg, S. Dapprich, A. D. Daniels, Ö. Farkas, J. B. Foresman, J. V. Ortiz, J. Cioslowski and D. J. Fox, Gaussian, Inc., Wallingford CT, 2013.

26 (*a*) T. Rajeshkumar, R. Jose, P. R. Remya and G. Rajaraman, *Inorg. Chem.*, 2019, **58**, 11927–11940; (*b*) M. M. Hänninen, A. J. Mota, R. Sillanpää, S. Dey, G. Velmurugan, G. Rajaraman and E. Colacio, *Inorg. Chem.*, 2018, **57**, 3683–3698.

27 (*a*) J. Cirera, Y. Jiang, L. Qin, Y. Z. Zheng, G. Li, G. Wu and E. Ruiz, *Inorg. Chem. Front.*, 2016, **3**, 1272; (*b*) K. R. Vignesh, S. K. Langley, K. S. Murray and G. Rajaraman, *Chem. – Eur. J.*, 2015, **21**, 2881–2892.

28 B. O. Roos, R. Lindh, P.-Å. Malmqvist, V. Veryazov, P.-O. Widmark and A. C. Borin, *J. Phys. Chem. A*, 2008, **112**, 11431–11435.

29 (*a*) S. Realista, A. J. Fitzpatrick, G. Santos, L. P. Ferreira, S. Barroso, L. C. J. Pereira, N. A. G. Bandeira, P. Neugebauer, J. Hrubý, G. G. Morgan, J. van Slageren, M. J. Calhorda and P. N. Martinho, *Dalton Trans.*, 2016, **45**, 12301–12307; (*b*) J. Li, R. M. Wei, T. C. Pu, F. Cao, L. Yang, Y. Han, Y. Q. Zhang, J. L. Zuo and Y. Song, *Inorg. Chem. Front.*, 2017, **4**, 114.

30 L. Noodleman, *J. Chem. Phys.*, 1981, **74**, 5737.

31 (*a*) A. D. Becke, *Phys. Rev. A*, 1988, **38**, 3098–3100; (*b*) A. D. Becke, *J. Chem. Phys.*, 1993, **98**, 5648–5652; (*c*) C. Lee, W. Yang and R. G. Parr, *Phys. Rev. B: Condens. Matter Mater. Phys.*, 1988, **37**, 785–789.

32 (*a*) M. K. Singh, *Dalton Trans.*, 2020, **49**, 4539–4548; (*b*) M. K. Singh and G. Rajaraman, *Inorg. Chem.*, 2019, **58**, 3175–3188; (*c*) M. K. Singh, T. Rajeshkumar, R. Kumar, S. K. Singh and G. Rajaraman, *Inorg. Chem.*, 2018, **57**, 1846–1858; (*d*) M. K. Singh, N. Yadav and G. Rajaraman, *Chem. Commun.*, 2015, **51**, 17732–17735; (*e*) A. Upadhyay, J. Rajpurohit, M. K. Singh, R. Dubey, A. K. Srivastava, A. Kumar, G. Rajaraman and M. Shanmugam, *Chem. – Eur. J.*, 2014, **20**, 6061–6070; (*f*) C. McDonald, S. Sanz, E. K. Brechin, M. K. Singh, G. Rajaraman, D. Gaynor and L. F. Jones, *RSC Adv.*, 2014, **4**, 38182; (*g*) S. Hazra, S. Bhattacharya, M. K. Singh, L. Carrella, E. Rentschler, T. Weyhermueller, G. Rajaraman and S. Mohanta, *Inorg. Chem.*, 2013, **52**, 12881.

33 T. R. Cundari and W. J. Stevens, *J. Chem. Phys.*, 1993, **98**, 5555–5565.

34 (*a*) A. Schaefer, H. Horn and R. Ahlrichs, *J. Chem. Phys.*, 1992, **97**, 2571; (*b*) A. Schaefer, C. Huber and R. Ahlrichs, *J. Chem. Phys.*, 1994, **100**, 5829; (*c*) G. E. Scuseria and H. F. Schaefer III, *J. Chem. Phys.*, 1989, **90**, 3700.

35 V.-A. Rassolov, J.-A. Pople, M.-A. Ratner and T.-L. Windus, *J. Chem. Phys.*, 1998, **109**, 1223–1229.